Proton and Zinc Effects on HERG Currents

Justus M. B. Anumonwo, Jorge Horta, Mario Delmar, Steven M. Taffet* and José Jalife
Departments of Pharmacology, and Microbiology and *Immunology, SUNY Health Science Center, 766 Irving Avenue, Syracuse, New York 13210

ABSTRACT The proton and Zn^{2+} effects on the human ether-a-go-go related gene (HERG) channels were studied after expression in *Xenopus* oocytes and stable transfection in the mammalian L929 cell line. Experiments were carried out using the two-electrode voltage clamp at room temperature (oocytes) or the whole-cell patch clamp technique at 35°C (L929 cells). In oocytes, during moderate extracellular acidification ($pH_o = 6.4$), current activation was not shifted on the voltage axis, the time course of current activation was unchanged, but tail current deactivation was dramatically accelerated. At $pH_o < 6.4$, in addition to accelerating deactivation, the time course of activation was slower and the midpoint voltage of current activation was shifted to more positive values. Protons and Zn^{2+} accelerated the kinetics of deactivation with apparent K_d values about one order of magnitude lower than for tail current inhibition. For protons, the K_d values for the effect on tail current amplitude versus kinetics were, respectively, 1.8 μM ($pK_a = 5.8$) and 0.1 μM ($pK_a = 7.0$). In the presence of Zn^{2+}, the corresponding K_d values were, respectively, 1.2 mM and 169 μM. In L929 cells, acidification to $pH_o = 6.4$ did not shift the midpoint voltage of current activation and had no effect on the time course of current activation. Furthermore, the onset and recovery of inactivation were not affected. However, the acidification significantly accelerated tail current deactivation. We conclude that protons and Zn^{2+} directly interact with HERG channels and that the interaction results, preferentially, in the regulation of channel deactivation mechanism.

INTRODUCTION

The delayed rectifier current (I_K) is a major repolarizing current in cardiac cells (McAllister et al., 1975; Campbell et al., 1992, Anumonwo et al., 1992; also reviewed in Gintant et al. 1992). In several species, I_K consists of two components with distinct biophysical and pharmacological properties (Sanguinetti and Jurkiewicz, 1990; Wang et al., 1993; Liu and Antzelevitch, 1995). One of these components, dubbed I_{Kr} for its rapid activation and rectification properties, is selectively inhibited by methanesulfonanilides (Sanguinetti and Jurkiewicz, 1990). The other component activates with relatively slower kinetics (hence termed I_{Ks}), has nonrectifying properties, and is insensitive to the methanesulfonanilides (Sanguinetti and Jurkiewicz, 1990). Human ether-a-go-go related gene (HERG) encodes a K^+ selective channel with biophysical and pharmacological properties nearly identical to I_{Kr} (Sanguinetti et al., 1995; Smith et al., 1996; Schönherr and Heinemann, 1996; Snyders and Chaudhary, 1996; Spector et al., 1996; Kiehn et al., 1996). There is evidence that the I_{Ks} channel results from the co-assembly of the KvLQT1 and the minK proteins (Barhanin et al., 1996; Sanguinetti et al., 1996).

Several reports have described the biophysical and pharmacological properties of HERG (Sanguinetti et al., 1995; Smith et al., 1996; Schönherr and Heinemann, 1996; Kiehn et al., 1996; McDonald et al., 1997; Zhou et al., 1998) and, in comparison, much less information is available in literature on HERG channel regulation. The modulatory effects of extracellular Ca^{2+} and Mg^{2+} on HERG channels were studied in *Xenopus* oocytes (Ho et al., 1998) and it was shown that both cations blocked the channels in a voltage- and time-dependent manner. In another important study, Paquette et al. (1998) investigated the effects of a group of transition metals (Cd^{2+}, Ni^{2+}, Co^{2+}, Mn^{2+}, and Zn^{2+}) on I_{Kr} in isolated rabbit ventricular myocytes. It was reported that the cations (Cd^{2+}, Ni^{2+}, Co^{2+}, Mn^{2+}) shifted current activation to the right on the voltage axis, increased the maximum current amplitude and accelerated current deactivation. Zn^{2+} decreased current amplitude but did not shift activation on the voltage axis. It was concluded that, whereas Zn^{2+} blocked the I_{Kr} channel, the other divalent cations altered rectification and/or inactivation mechanisms of the channel.

Ion channel function is altered by the hydrogen concentration in the cellular environment (reviewed in Hille, 1992). In the heart, myocardial ischemia results in a variety of metabolic changes, ultimately leading to the acidification of the cellular environment (for a review see Cascio et al., 1995). The reduction in pH has been shown to adversely affect the conduction and excitability properties of the cardiac muscle (Hille, 1992; Cascio et al., 1995), effects that have been attributed to proton-induced changes on ion channel properties (Kurachi, 1982; Yatani et al., 1984; Krafte and Kass, 1988; Zhang and Siegelbaum, 1991; Watson and Gold, 1995). To our knowledge, there is no report in the literature on proton effects on the HERG channel. In this study, therefore, we have investigated the effects of extracellular protons as well as zinc on HERG channels after

Received for publication 17 July 1998 and in final form 9 April 1999.

Address reprint requests to Justus M. B. Anumonwo, Ph.D., Department of Pharmacology, SUNY Health Science Center, 766 Irving Avenue, Syracuse, NY 13210. Tel.: 315-464-7990; Fax: 315-464-8014.

This work was supported by grants from the National Institutes of Health (PO1-HL39707) and the New York State Affiliate of the American Heart Association (Grant-in-aid to J.M.B.A. and Fellowship to J.H.).

0006-3495/99/07/282/17 $2.00

expression in *Xenopus* oocytes and stable transfection in mammalian (L929) cells. It has been shown previously that Zn^{2+} interacts with potassium channels in a manner similar to protons (Gilly and Armstrong, 1982; Coulter et al., 1995, De Biasi et al., 1993). Part of this work has been presented previously in abstract form (Horta et al., 1996).

MATERIALS AND METHODS

Oocyte preparation and injection of cRNA

Experiments were performed on stage V or VI *Xenopus laevis* oocytes. *X. laevis* frogs were anesthetized by immersion in 0.2% MS-222 (3-aminobenzoic acid ethyl ester). Oocytes were surgically removed and placed in Leibovitz L-15 (0.5X) culture medium, with L-glutamine and without Na_2CO_3 (GIBCO BRL Life Technologies, Inc.). The medium was prepared as instructed by the supplier, with 25 mM HEPES (pH 7.4), 10 mg/mL streptomycin, 25 mg/mL amphotericin B, and 10,000 U of penicillin. Oocytes were digested with 5 mg/mL type 1A collagenase in L-15 for 2–2.5 hr. After washing off the enzyme, the residues in the external envelopes of the oocytes, except the vitelline layer, were removed using fine forceps. To prevent contamination from an oocyte endogenous current (connexin38 hemi-gap-junction channels; Ebihara, 1996), the oocytes were injected with 50 ng of antisense for Cx38 (see Barrio et al., 1991). One day after Cx38 antisense injection, the oocytes were injected with 30 ng of HERG-cRNA (cDNA was kindly provided by Dr. M. Keating of Eccles Institute of Human Genetics, Salt Lake City, UT). Transcription was carried out using mMESSAGE mMACHINE kit (Ambion). In all experiments, oocytes were injected with a 50-nL mixture of cRNA (0.6 μg/μL) and the dextran form of a proton-sensitive dye, seminaphthorhodafluor (SNARF) (MW 70,000; Molecular Probes Inc.).

Transfection and cell culture

The coding region of HERG cDNA was subcloned into the mammalian expression vector pCDNA3 (Invitrogen, San Diego, CA) for transfection into cells. The L929 cell line was obtained from American Tissue Cell Culture (CCL-1) and grown in Dulbecco's modification of Eagle's medium (DMEM) with penicillin (100 U/mL), streptomycin (100 μg/mL), HEPES (25 mM), and fetal bovine serum (10%). Transfection of HERG into L929 cells was achieved by the lipofectin method (Life Technologies, Grand Island, NY). Transfected clones were initially selected by 800 μg/mL G418, and then further selection was done using 2400 μg/mL of G418. Transfectants were kept in DMEM. Cells were subcultured into 35 $\times$ 10 mm Corning disposable sterile tissue culture dishes (Corning, NY). Control experiments were performed in nontransfected cells.

Electrophysiology

Two-electrode voltage clamp

After preparation and injection, oocytes were placed in culture dishes and subsequently transferred to the stage of an inverted microscope (Nikon Diaphot, model 200, Melville, NY) equipped for carrying out optical measurements of intracellular pH (see below). To visualize oocytes during impalement, we used a separate stereomicroscope (Nikon, model SMZ-1S). HERG currents were recorded at room temperature (21–23°C) using the standard two-microelectrode voltage-clamp technique. Electrodes were filled with 3 M KCl and had resistances of 2–5 MΩ for voltage-recording electrode and 0.5–0.9 MΩ for the current-passing electrode.

Whole-cell patch-clamp

Suction pipettes were fabricated from glass capillaries purchased from World Precision Instruments, Inc., New Haven, CT; glass IBBL W/Fil (1B120F-4). Pipettes were pulled using a two-stage puller (Sutter Instrument Co, Novato, CA; model P-30) and were gently heat-polished using a microforge (model MF-83; Narishigi, Tokyo, Japan). When filled with internal filling solution, the pipettes had a resistance in the range of 2–3 MΩ.

Electrophysiology was commenced 24–48 h after plating of cells in the tissue culture dishes. The culture dishes were transferred to the stage of an inverted microscope (Nikon Diaphot; Nikon, Melville, NY) equipped with a temperature control unit (OPMI, Medical systems, Greenvale, NY), and appropriate solutions were gravity fed onto the cells in the dishes and maintained at 35 $\pm$ 0.5°C for the electrophysiology. Recordings were carried out using an Axopatch 1D amplifier (Axon Instrument, Forest City, CA) as previously described (Hamill et al., 1981; Anumonwo et al., 1990). Briefly, the suction pipette was lowered into the external solution and the junction potential nulled. The pipette was then advanced until contact with a cell for seal formation. After seal (5–40 GΩ) formation and patch break, cell resting membrane potential was recorded and the cell capacitance and input resistance were determined from capacitive current spikes elicited following symmetrical application of 10 mV from a holding potential of -100 mV. Subsequently, cell capacitive currents and series resistance were optimally ($\sim$80%) compensated. Leak and capacitive current subtraction was carried out online using the standard P/3 paradigm.

Solutions

Oocytes

Extracellular acidification. Experiments were carried out in ND96 solution (see Sanguinetti et al., 1995) adjusted to the appropriate pH values. The external solution contained (in mM): NaCl, 96; KCl, 2; MgCl, 1; $CaCl_2$, 0.4; $MnCl_2$, 2; and either MES, 5 (pH = 5.0 $-$ 6.5), HEPES, 5 (pH = 7.0 $-$ 8.0), or Tris, 5 (pH = 8.5 $-$ 9.0). pH values were adjusted using HCl or NaOH just before experiments. During experimentation, oocytes were exposed to ND96 solutions buffered to the various pH values, in 0.5 pH unit steps. To enable equilibration at each pH value, the volume of the recording chamber was exchanged about seven times at each pH examined, and each oocyte was exposed to the range of pH values examined. To determine the effect of extracellular Zn^{2+}, solutions containing different concentrations of Zn^{2+} were adjusted to a pH of 7.4. Compensation for osmolarity was carried out only for the 10 mM Zn^{2+}-containing solution, in which the NaCl was reduced to 81 mM.

L929 cells

The external (control) solution contained (in mM): 142 NaCl, 5.4 KCl, 1 $CaCl_2$, 6 Glucose, and 10 HEPES, at pH 7.4. The intracellular (pipette) solution contained (in mM): 153 KCl, 1 $MgCl_2$, 10 HEPES, 5 EGTA, and 2 sodium ATP (added daily), at pH 7.2. In K^+ selectivity experiments, external potassium was changed to 1, 5.4, and 10 mM. Osmolarity compensation was carried out only at $[K^+]_o$ = 10 mM, with equimolar substitution of extracellular Na.

Extracellular acidification. As stated previously, our objective in this study was to examine the effect of relatively moderate extracellular acidification on HERG currents. To acidify the extracellular space, the pH of the external solution was lowered by one pH unit to 6.4 from the control value of 7.4. The control solution was buffered to 7.4 using HEPES (pK_a = 8.0) and the solution during acidification was buffered to 6.4 using MES (pK_a = 6.1). In all experiments, the pH of the intracellular pipette solution was kept at 7.2.

Chemical compounds for cell culture and for the preparation of the stock solutions were purchased from Sigma Chemical Company, St. Louis, MO. E-4031 (1-[2-(6-methyl-2-pyridyl)ethyl]-4-(4-methyl-sulfonylaminobenzoyl) piperidine dihydrochloride) was a gift of the Eisai Co., Ltd. Tsukuba Research Laboratories, Ibaraki, Japan. To test the E-4031 sensitivity on HERG currents, appropriate amounts of the stock solutions were added to the external solution during experiments.

Measurements of intracellular pH

Intracellular pH (pH_i) measurements were carried out optically, using a video camera-based fluorescence ratio imaging system (C-Imaging, model 1280, Mars, PA). SNARF was used to determine the intracellular pH in oocytes (Morley et al., 1996). SNARF is a single-excitation (534 nm) dual-emission (590 nm, 640 nm) fluorophore. Oocytes were injected with 50 nL of a 350 μM solution of SNARF. Intracellular concentration of the dye was approximately 17 μM. Light excitation and optical recordings were carried out from the bottom of the preparation, using the 10X objective of the inverted microscope. The SNARF-loaded oocytes were illuminated with a Xenon arc lamp and emission was monitored at two selected wavelengths (590 nm and 640 nm). The emission filters were mounted on a wheel at the side arm of the Nikon inverted microscope. The filter wheel device cycled between the two selected emission filters with a frequency of 33.3 Hz. The recorded wavelengths were passed through an image intensifier, which provided low light amplification before image acquisition by a Daga MTI CCD-725 series camera. Both the camera and the image intensifier were directly connected to a GEN II SYS unit, which controlled the camera shutter and the intensity settings of the image intensifier. Optical signals received by the camera were digitized and visualized in real time as well as stored in a computer.

To estimate intracellular pH, emission ratios were compared with those recorded with a SPEX Fluorolog system that is available in our laboratory. The calibration of the latter system has been previously described (Morley et al., 1996). As expected, there was a linear relationship between the emission ratios obtained from both systems for measurements within the dynamic range of the dye (Ek-Vitorin et al., 1996).

Data acquisition and analysis

Acquisition and analysis of data were carried out using a commercially available software (pCLAMP, version 6; Axon Instrument, Forster City, CA) installed on a pentium-based computer. Current signals were filtered (−3 db; 4-pole Bessel filter, LPF 202; Warner Instrument Corporation, Hamden, CT) and digitally sampled at a rate equal to two to four times the low pass cutoff frequency, and was usually 1.61 kHz in the oocyte experiments. For experiments in L929 cells that were carried out at 35°C, traces were sampled at 5–50 kHz, depending on the experiment. To resolve tail currents during acidification experiments, we used a split-clock sampling procedure with faster acquisition (up to 20 kHz) during the initial decline of tail currents.

Current amplitude

The amplitude of tail currents was estimated either from the peak amplitude of the tail current or, where indicated, extrapolating the exponential function back to the beginning. Data of tail current amplitude versus voltage were fitted with a Boltzmann function,

$$I(V) = 1/\{1 + \exp[(V_{1/2} - V_t)/k]\}, \quad (1)$$

where I is the relative tail current, $V_{1/2}$ is the voltage required for half activation of current, V_t is the test potential, and k is the slope factor.

To determine cation (H^+ or Zn^{2+}) sensitivity of HERG, we fitted the data of fractional tail current at −60 mV (test pulse = +40 mV) as a function of extracellular cation concentration with the Hill equation,

$$I = 1/\{([C]/pK_d)^n + 1\}, \quad (2)$$

where K_d is the acid constant, n is the Hill coefficient, and $[C]$ is the cation concentration.

Current kinetics

Pulse and tail currents were fitted with the appropriate biexponential functions available in the Clampfit subroutine of the pCLAMP software. The kinetics of current activation were studied using two methods. First, apparent activation was determined by directly fitting the pulse current to a biexponential function (at 0 mV). It has been previously shown that, at voltages ≤0 mV, directly fitting pulse currents yields reasonable estimates of current activation (Zhou et al., 1998). The second method was used in the L929 cells, and involved measuring the time course of pulse current amplitude in an envelope (at +60 mV). Each current amplitude in the envelope was measured after a brief hyperpolarizing prepulse to remove current inactivation (see Results). A plot was then generated for the current amplitudes as a function of time, and fitted to a single exponential function,

$$Y = Y_0 + Ae^{-(x-x_0)/\tau}, \quad (3)$$

where X_0 is the X value offset, Y_0 is the Y value offset, A is amplitude, and τ is the time constant that describes current activation. To analyze the kinetics of current deactivation, tail currents were fitted using a double exponential function available in the pClamp software. To determine the kinetics of channel inactivation, current traces generated using the appropriate voltage-clamp protocols were fitted to either a single (onset of inactivation) or a double (recovery from inactivation) exponential function. Recovery kinetics were analyzed by examining the fast time constant of the double exponential function (Spector et al., 1996).

To determine the K_d for the effect on current deactivation kinetics, tail currents at −60 mV (test pulse to +40 mV) were fitted to biexponentials, and the time constants were plotted as functions of extracellular cation concentration. The curves were fitted with a form of the Hill equation (see Coulter et al., 1995),

$$\tau/\tau_{max} = A*1/\{([C]/K_d)^n + 1\} + \tau_o, \quad (4)$$

where τ represents time constants and A is a (variable) fitting parameter.

K^+ selectivity

K^+ selectivity was determined by fitting the plot of E_{rev} versus $[K^+]_o$ to the Goldmann–Hodgkin–Katz equation (Goldmann, 1943; Hodgkin and Katz, 1949),

$$E_{rev}(mV) = 61 \log\left(\frac{\alpha[Na^+]_o + [K^+]_o}{\alpha[Na^+]_i + [K^+]_i}\right), \quad (5)$$

where α is the relative permeability of Na^+ to K^+ (determined from the fitting procedure), $[Na^+]_o$ = 142 mM, and $[K^+]_i$ = 153 mM.

Estimation of charge density

Charge density was estimated (see Elinder et al., 1996; Zhou and Jones, 1996) using the Grahame (1947) equation,

$$\sigma_f^2 G^2 = [C_i]\{\exp(-z_i\varphi F/RT) - 1\}, \quad (6)$$

where σ_f is free surface charge density, C_i is the concentration of the ith ion and z_i its valence, φ is the surface potential, F is the Faraday constant, R is the gas constant, T is the absolute temperature, and G is a constant equal to 270 $Å^2e^{-1}M^{1/2}$ at room temperature. A conjugate gradient method (Bard, 1974) with inherently rapid convergence, was used to fit the data to obtain the parameters (pK_a and σ; see Zhou and Jones, 1996).

Statistical analyses among groups were made using one-way analysis of variance (ANOVA), and differences between subgroups were determined using the Bonferroni correction. We used the Student's t-test to evaluate differences between paired observations. We considered p values of < 0.05 as significantly different. Data are expressed as the mean ± SE (n = number of oocytes).

RESULTS

For the sake of clarity, the experimental results of cation effects in *Xenopus* oocytes and in the L929 cells are pre-

sented sequentially. Although we investigated proton and Zn^{2+} effects on HERG channels in oocytes, only proton effects were determined in the L929 cells. In both expression systems, the focus of our investigations was on cation effects on voltage-dependent activation, suppression of tail current amplitude and the kinetics of current activation/deactivation.

Proton and zinc effects on HERG channels in *Xenopus* oocytes

Control experiments were carried out to ascertain that oocytes injected with HERG cRNA, SNARF, and Cx38 antisense expressed currents with properties similar to those previously reported for HERG. In voltage-clamp experiments (protocol in Fig. 1), HERG pulse currents peaked at approximately 0 mV, whereas the tail currents saturated at voltages beyond +20 mV (for example, see control data in Fig. 1). A Boltzmann function fit of the voltage dependence of current activation yielded $V_{1/2} = -8.4 \pm 1.0$ mV and $k = 8.5 \pm 0.3$ mV in the control experiments ($n = 10$). Results from these experiments showed that current activation and rectification under these conditions were similar to those previously reported for HERG (Sanguinetti et al., 1995).

Voltage-dependent activation

To study proton effects on voltage-dependent activation, 4-sec depolarizing pulses (holding potential (HP) = −60 mV) were applied starting from −50 mV to progressively more positive potentials in 10-mV increments. Tail currents were recorded on the return of membrane potential to −60 mV. In Fig. 1 *A* are representative traces obtained from one oocyte showing HERG currents with a voltage pulse (V_P) = +20 mV in control ($pH_o = 7.4$) and during acidification to $pH_o = 5.8$. (K_d for proton effect on tail current amplitude = 5.8 [see later]). Acidification caused a significant inhibition of pulse (I_P) and of tail (I_T) currents by 50% and 63%, respectively. As is evident in the time course of current traces, the acidification also affected current kinetics. The pH effects on current kinetics will be addressed in a later section. The acidification effects on the voltage-dependent activation of HERG are summarized in Fig. 1 *B* for I_P and in Fig. 1 *C* for I_T ($n = 5$). Note that current amplitudes at $V_p > +40$ mV were greater than their corresponding control values, which may reflect an effect of protons on channel rectification (Paquette et al., 1998). The voltage dependence of channel activation (Fig. 1 *C*) was significantly shifted on the voltage axis by ~+19 mV compared to control values. However, the acidification had no significant effect on *k*. In a separate set of experiments, we investigated the effect of relatively moderate acidification ($pH_o = 6.4$) on HERG. Although the voltage-dependence of channel activation was not shifted by the acidification, there was ~11% inhibition of I_T (data not shown; however, see experiments in L929 cells in a later section).

To determine extracellular Zn^{2+} effects on HERG channels, pH_o was kept constant at control (7.4) values, and intracellular pH was monitored to ensure its stability. The general effects of the divalent cation are illustrated in Fig. 2. The voltage-clamp protocol used was similar to that in Fig. 1. Figure 2 *A* illustrates currents in control and during Zn^{2+} superfusion. The extracellular Zn^{2+} effects were reversible (data not shown). Zn^{2+} effects in five experiments are summarized in Fig. 2 *B* for I_P and in Fig. 2 *C* for I_T. In these experiments, current activation was shifted by approximately +21 mV and there was no significant zinc effect on *k*.

To gain further insight into proton and Zn^{2+} effects, we measured current activation with H^+ and Zn^{2+} simultaneously present in the external solution. First, current activation was determined in control and at $pH_o = 5.8$ (same protocol as in Fig. 1). The oocytes were then exposed to an acidified zinc solution. This was a solution at low pH_o (pH = 5.8), which also contained 1.2 mM Zn^{2+} (1.2 mM was the K_d determined for Zn^{2+} inhibitory effect on HERG tail current amplitude; see Fig. 4 *C*). In four oocytes, tail currents were inhibited by approximately 44% at $pH_o = 5.8$ and by 64% in the presence of $pH_o = 5.8$ plus Zn^{2+} (Fig. 3 *A*). The amount of block is comparable to the 65–70% block recorded at about twice the K_d for the cations (in Fig. 4, *A* and *C*). As shown in Fig. 3 *B*, current activation was shifted by +17 mV during exposure to the low pH solution alone and by a total of +26 mV during exposure to the acidified Zn^{2+} solution.

Zn^{2+} and proton effects on a variety of K^+ channels are thought to involve surface charge screening and/or specific interaction of the cations with sites on the channel (Gilly and Armstrong, 1982; Agus et al., 1991; De Biasi et al., 1993; Paquette et al., 1998). In fact, it has been suggested that Zn^{2+} and protons may bind to identical, negatively charged sites on the K channel (Coulter et al., 1995). To estimate the density of such charges, we used an approach similar to that described previously for other cloned K^+ channels (Elinder et al., 1996). The voltage protocol used was the same as described for the measurement of voltage-dependent activation. The shift in current activation at a given pH_o was measured as the shift in $V_{1/2}$ relative to that of the control value, i.e., at $pH_o = 7.4$, and are presented in Fig. 3 *C*. The open circles in the plot represent data measured from individual experiments. Extracellular acidification caused a maximum shift of approximately 25–30 mV at $pH_o = 5.0$. An estimation of charge density (at $pH_o = 7.4$) was made by fitting the data points to the Grahame equation, with $\sigma = -1e/425$ Å^2 and pK_a of 5.5 (*solid line* in the figure). Note that there was no significant shift in the midpoint voltage of activation in the range of $pH_o = 6.5$ and 8.0. Also, the total predicted shift (~25–30 mV) is approximated by the combined amount of shift during the simultaneous presence of protons and Zn^{2+} (Fig. 3 *B*).

Current amplitude

Proton effects on current amplitude were determined by measuring I_T inhibition at a range of proton concentrations ($[H^+] = 10^{-8} - 10^{-5}$ M). After equilibration at each $[H^+]$

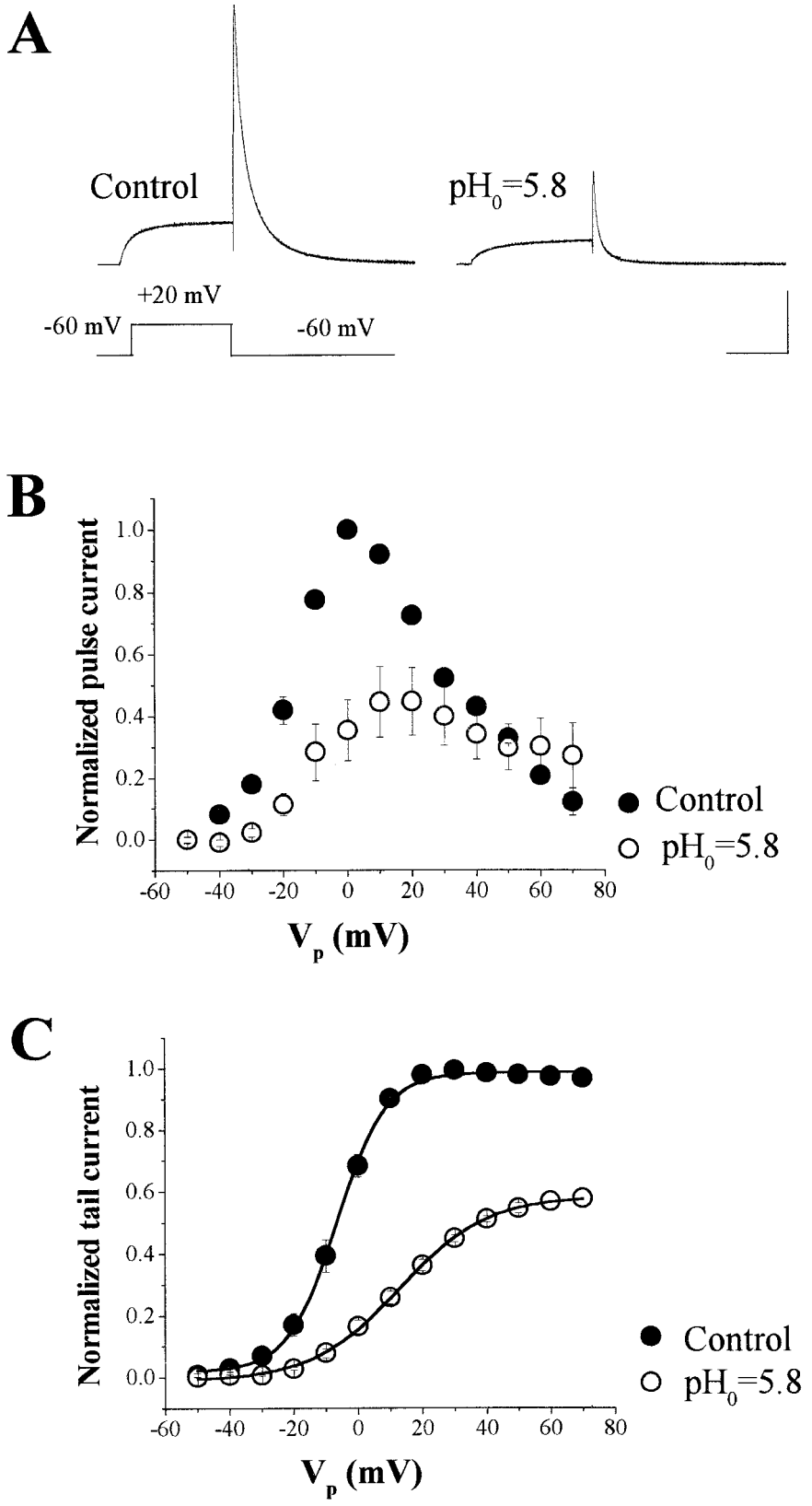

FIGURE 1 Effects of extracellular acidification on HERG currents in oocytes. (*A*) Current traces obtained in control (pH_o = 7.4; *left*) and during acidification to 5.8 (*right*). The currents were recorded from the same oocyte and were activated by 4-sec voltage clamp steps. Calibration bars: 0.5 μA, 2 sec for both current traces. (*B*) pH_o (5.8) effects on pulse currents. (*C*) pH_o (5.8) effects on tail currents. In *B* and *C*, test currents were normalized to their respective control values. Individual experiments were fitted using the Boltzmann function; $V_{1/2}$ and k, respectively, were -5.3 ± 2.2 mV and 8.0 ± 0.3 mV in control and were 13.3 ± 3.2 mV, and 12.5 ± 0.7 mV during acidification (n = 5).

value (see Methods), tail currents recorded at -60 mV ($V_p = +40$ mV) were normalized to the value at $[H^+] = 10^{-8}$ M and plotted as a function of $[H^+]$ (Fig. 4 *A*). There was virtually no change in I_T at $[H^+]$ values lower than 10^{-6} M; however, at higher values, I_T was significantly decreased. The proton effect on I_T was reversible (data not shown). The data were fitted to the Hill equation with a K_d of 1.8 ± 0.3 μM (pK_a of 5.8 ± 0.1) and a Hill coefficient

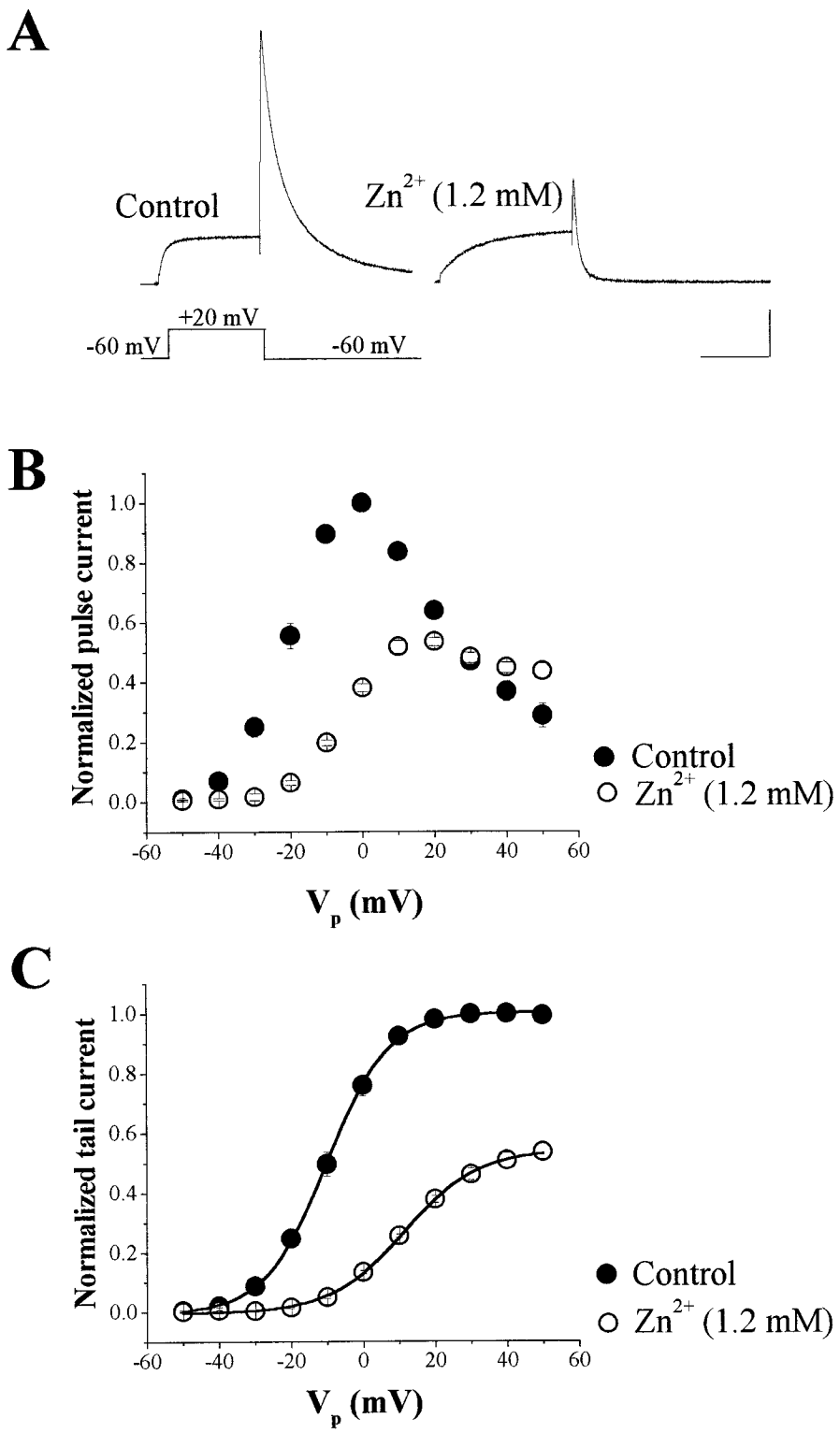

FIGURE 2 Effects of extracellular Zn^{2+} (1.2 mM) on HERG currents in oocytes. (*A*) Current traces obtained in control external solution and in the presence of Zn^{2+}. The currents were recorded from the same oocyte and were activated by 4-sec voltage clamp steps. Calibration bars: 0.5 μA, 2 sec for both current traces. (*B*) Effects of Zn^{2+} on pulse currents. (*C*) Effects of Zn^{2+} on tail currents. Individual experiments were fitted using the Boltzmann function; $V_{1/2}$ and k, respectively, were -10.2 ± 1.5 mV and 8.3 ± 0.1 mV in control and were 11.1 ± 1.1 mV, and 9.8 ± 0.3 mV in the presence of Zn^{2+} ($n = 5$).

of 1.2 ± 0.1 ($n = 8$). To rule out the possibility that the changes in extracellular $[H^+]$ altered intracellular $[H^+]$ in the experiments shown in Fig. 4 *A*, we carried out simultaneous measurements of intracellular pH in the experiments. As shown in Fig. 4 *B*, there was no significant change in intracellular pH during the approximately 50-min period of changing extracellular $[H^+]$ from 10^{-8} to 10^{-5} M. The intracellular pH averaged 7.6 ± 0.02 at the beginning of the experiment and 7.5 ± 0.03 at the end of the acidification challenge ($n = 6$).

HERG is modulated by extracellular K^+ concentration ($[K^+]_o$), and the current amplitude is increased in direct proportion to $[K^+]_o$. Sanguinetti et al. (1995) showed that HERG current amplitude in 2 mM $[K^+]_o$ was less than 50%

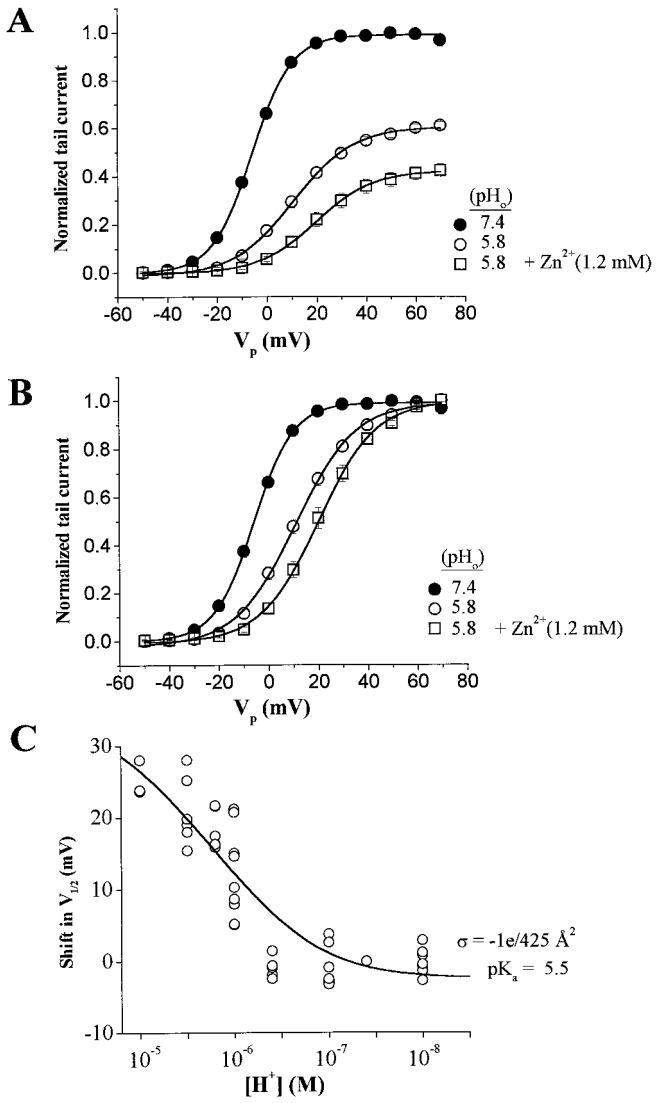

FIGURE 3 Proton and Zn^{2+}-induced shifts in voltage-dependent activation in oocytes. (*A*) Effects of acidification (pH_o = 5.8) with and without Zn^{2+} (1.2 mM) on tail current amplitude (n = 4). Data were normalized to the maximum control values. (*B*) Cation-induced shifts in midpoint voltage of channel activation by acidification (pH_o = 5.8) with and without Zn^{2+} (1.2 mM); n = 4. Each data set was normalized to its maximum value. (*C*) Proton concentration-dependent shift in channel activation. Voltage-dependent activation was measured as in previous figures. The shift in activation at a given pH_o was determined as a shift in $V_{1/2}$ relative to the control (pH_o = 7.4) value of $V_{1/2}$. The solid line represents the fit with the Grahame equation. Charge density = $-1e/425$ Å^2 and pK_a = 5.5 (n = 3–9).

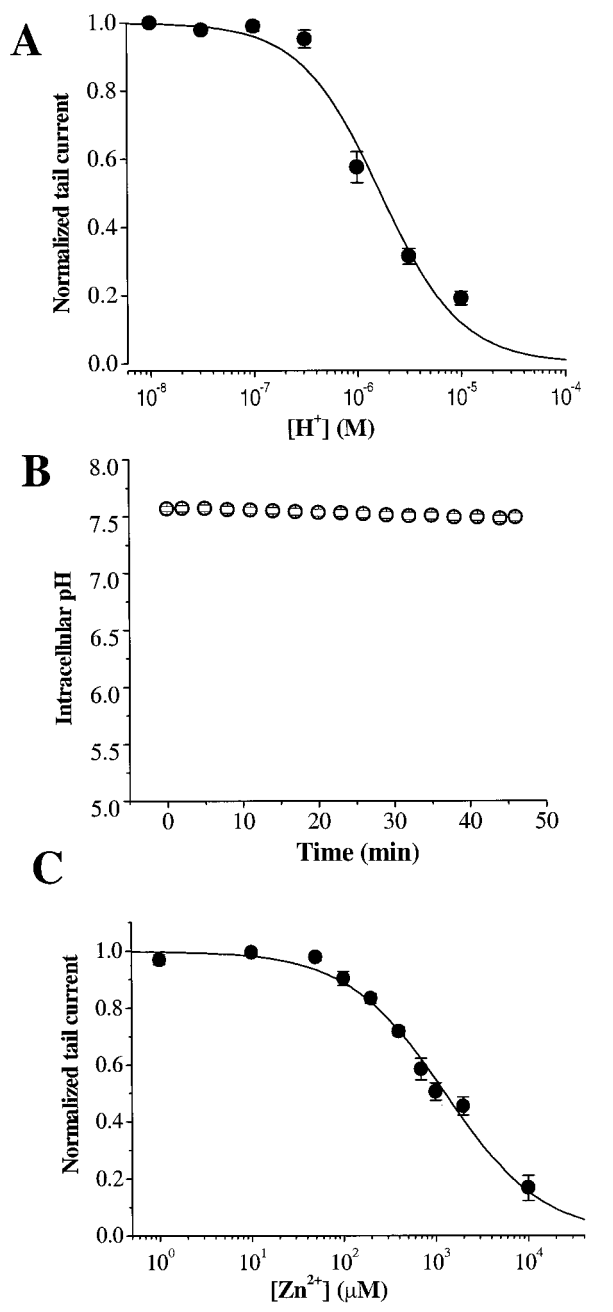

FIGURE 4 Cation concentration-dependent effects on HERG tail current amplitude in oocytes. (*A*) Inhibition of tail currents by protons. Tail current amplitude was measured at −60 mV (V_p = +40 mV) at each concentration and normalized to the amplitude at $[H^+] = 10^{-8}$ M. Data from each oocyte were plotted and fitted to the Hill equation. K_d = 1.80 ± 0.25 μM (pK_a 5.80 ± 0.05) with a Hill coefficient of 1.18 ± 0.06 (n = 8). The line is the best fit of averaged data. (*B*) Lack of a significant change in intracellular pH during extracellular pH changes. Data are simultaneous intracellular pH measurements taken from six oocytes in (*A*). Intracellular pH was monitored every 1 min, but some datapoints have been removed for clarity. Intracellular pH values were 7.6 ± 0.02 at the beginning of the experiment ($[H^+]_o = 10^{-8}$) and 7.5 ± 0.03 at the end of the experiment ($[H^+]_o = 10^{-5}$). (*C*) Inhibition of tail currents by Zn^{2+}. Tail currents were recorded using the same protocol as shown in *A* and were normalized to the maximum control value for each cell. The line is the best fit of averaged data to a Hill equation. K_d = 1.2 ± 0.10 mM and the Hill coefficient = 0.96 ± 0.05 (n = 7).

of the amplitude when $[K^+]_o$ was 5 mM. Given that our experiments on pH_o effects on current amplitude were carried out in the presence of 2 mM $[K^+]_o$, in a separate set of experiments, we examined acidification effects at $[K^+]_o$ = 10 mM (n = 4). In these experiments analyses were carried out on I_P because, given the voltage-clamp protocol and the $[K^+]_o$, I_T measurements were not possible. At $[K^+]_o$ = 10 mM, inhibition of peak I_P was 38 ± 3%, i.e., approximately 17% less than at $[K^+]_o$ = 2 mM. These data suggest an

interaction between extracellular potassium ions and protons on the HERG channel.

The concentration dependence of extracellular Zn^{2+} effect on I_T is shown in Fig. 4 *C*. In seven oocytes, I_T values measured at −60 mV (V_p = +40 mV) were normalized to the maximum I_T and plotted against external Zn^{2+} concentrations. The data were fitted to the Hill equation, with a K_d of 1.2 ± 0.1 mM, and a Hill coefficient of 0.96 ± 01.

Current activation/deactivation

We measured the effects of changes in extracellular proton concentration on the time course of current activation/deactivation. As previously pointed out, HERG channel activation and deactivation are strongly influenced by a rapid inactivation process. Therefore, the time constants obtained by exponentially fitting pulse and tail currents as described below, only reflect macroscopic changes in the time course of HERG currents, and should be regarded as effects on *apparent* activation/deactivation of the channel. Proton effects on kinetics of current activation were studied by fitting I_P at 0 mV in control and during acidification (to 6.4 and 5.8) (see Table 1).

HERG current activation was not significantly altered by acidification to 6.4; however, lowering pH_o to 5.8 significantly slowed down activation (Table 1; also, see I_P in Fig. 5 *A*). The slowing effect at pH_o = 5.8 was reflected as an increase in the time constant of the slow component of current activation. In contrast to these effects on activation, acidification significantly accelerated I_T deactivation at both pH_o values (Table 1). Representative traces with superimposed fits (I_T only) are shown in Fig. 5 *A*. The plots in Fig. 5 *B* illustrate the voltage-dependence of the acidification effects on the time constants of current deactivation. Note that, compared to control conditions, acidification altered the voltage-dependence of the fast and slow time constants (τ_f, τ_s), as shown by the change in the shape of the curves. During acidification, the relative amplitude of the fast component at −40 mV was significantly different from control values, respectively, 0.3 ± 0.01, 0.7 ± 0.05 (n = 5) but was unchanged at more negative potentials (−50 to −90 mV). The dramatic proton effect on current deactivation prompted us to investigate the sensitivity of the deactivation process to proton concentration (Fig. 5 *C*). Tail currents at −60 mV (V_p = +40 mV) were fitted biexponentially, and the time constants were normalized to the value at $[H^+] = 10^{-9}$ M and then plotted against extracellular proton concentration. The data were fitted to a Hill equation with K_d of approximately 0.10 μM (pK_a = 7.03; fast component). These data show that, compared to current inhibition, HERG current deactivation is about one order of magnitude more sensitive to proton concentration in the cellular environment.

We carried out similar analysis on extracellular Zn^{2+} effects on HERG current deactivation (Fig. 6 and Table 1). Representative traces, with superimposed biexponential fits (I_T only), in control and in the presence of extracellular Zn^{2+} are shown in Fig. 6 *A*. Fig. 6 *B* illustrates the voltage-dependence of the Zn^{2+} effects on τ_f and τ_s. Note that, as was shown for protons, Zn^{2+} also changed the shape of the τ–V curves. In the presence of Zn^{2+}, the relative amplitude of the fast component at −40 mV was different from control values, respectively, 0.4 ± 0.01, 0.9 ± 0.1 (n = 4), and was also unchanged at more negative potentials (−50 to −90 mV). As was determined for protons, the Zn^{2+} sensitivity of I_T deactivation was investigated at −60 mV (V_p = +40 mV). The time constants of I_T deactivation were fitted biexponentially and plotted against extracellular Zn^{2+} concentrations (Fig. 6 *C*). The K_d for Zn^{2+} effect was 169 μM (fast component). Note that this K_d is also about one order of magnitude less than for the inhibitory effect of extracellular Zn^{2+} on the tail currents.

Proton effects on HERG in L929 cells

To better understand the physiological implications of the proton effects on HERG, we carried out stable transfection of HERG channels in the mammalian L929 cells and tested the effects of relatively moderate acidification (pH_o = 6.4). We examined proton effects on the voltage-dependent activation, the kinetics of activation/deactivation, and the onset and recovery of inactivation. HERG channels had been previously expressed in HEK cells (Zhou et al., 1998) and in CHO cells (McDonald et al., 1997). After stable transfection in the L929 cells, we profiled HERG channel biophysical and pharmacological characteristics.

TABLE 1 Kinetics of activation/deactivation

	Activation (0 mV)		Deactivation (−60 mV)		
	pH_o = 6.4 (Control/Test)	pH_o = 5.8 (Control/Test)	pH_o = 6.4 (Control/Test)	pH_o = 5.8 (Control/Test)	$[Zn^{2+}]$ = 1.2 mM (Control/Test)
τ_{fast}	0.33 ± 0.02	0.30 ± 0.02	0.59 ± 0.06	0.64 ± 0.04	0.49 ± 0.06
(sec)	0.30 ± 0.01	0.32 ± 0.01	0.23 ± 0.02*	0.10 ± 0.01*	0.10 ± 0.00*
τ_{slow}	2.10 ± 0.2	1.97 ± 0.07	2.63 ± 0.31	3.20 ± 0.25	1.87 ± 0.28
(sec)	1.62 ± 0.9	2.82 ± 0.11*	1.20 ± 0.08*	0.45 ± 0.03*	0.41 ± 0.02*
n	9	5	9	5	4

Currents were activated by 4-sec depolarization to 0 mV (V_p). Holding potential = −60 mV. Data are expressed as means ± SE; n, number of observation.
*Significant difference compared to control; $p < 0.05$.

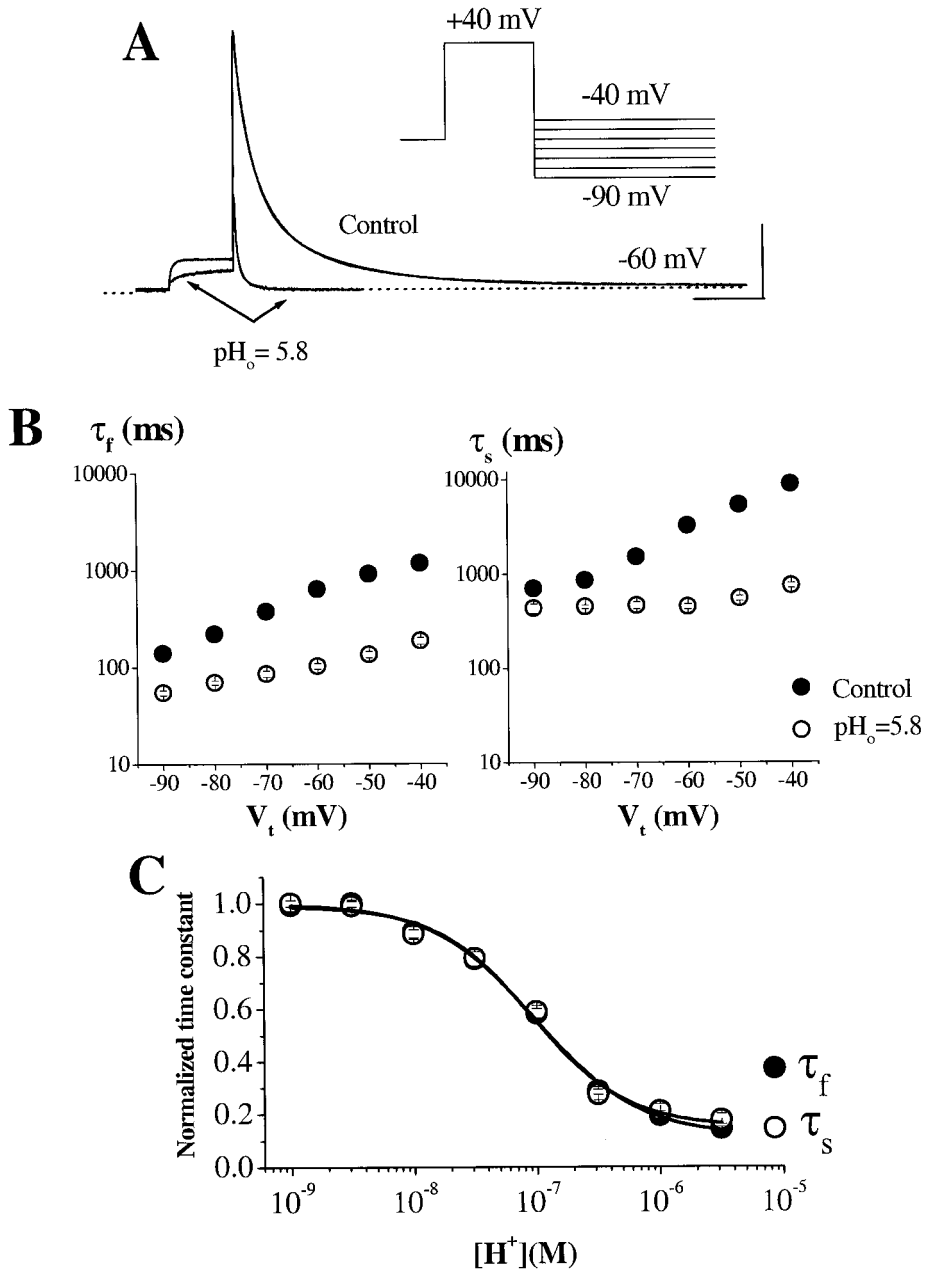

FIGURE 5 Effects of acidification (pH_o = 5.8) on tail current deactivation kinetics in oocytes. (*A*) Representative traces in control and during acidification. The tail current was recorded at −60 mV (V_t) after 2-sec depolarization steps to +40 mV. Note the faster deactivation of tail current during acidification. In this and the next figure, tail current duration at pH_o = 5.8 is shorter to enable a faster sampling rate (20 kHz). Tail currents in control and during acidification have superimposed biexponential fits with time constants of 0.54 and 2.59 sec in control and 0.08 and 0.40 sec during acidification. Calibration bars: 1 μA, 2 sec. (*B*) Voltage dependence of the fast (τ_{fast}; *left plot*) and the slow (τ_{slow}; *right plot*) time constants (n = 5). (*C*) The time constants (τ_{fast}, τ_{slow}) of tail current deactivation plotted as a function of extracellular proton concentration. The lines represent the best fit of data to a modified Hill equation (in Materials and Methods). The K_d values for τ_{fast}, τ_{slow}, respectively, were 0.10 ± 0.01 μM and 0.09 ± 0.01 μM (pK_a values = 7.03 and 7.07), with Hill coefficients, respectively, of 1.07 ± 0.07 and 1.22 ± 0.12 (n =5).

Properties of stably transfected HERG channels

L929 cells stably transfected with HERG had a resting membrane potential of −39 ± 1.7 mV, cell capacitance of 21.9 ± 1.6 pF and input resistance of 1.3 ± 0.3 GΩ (n = 14). Representative HERG current traces in the transfectants are shown in Fig. 7 *A*. Currents were activated by 4-sec depolarizing pulses in 10-mV increments (protocol shown as inset). The relatively large tail currents are each preceded by a hook, reflecting the channel recovery from the inactivated state (Sanguinetti et al., 1995; Snyders and Chaudhary, 1996). Nontransfected L929 cells subjected to an identical voltage-clamp protocol had no similar time-dependent currents (lower traces in Fig. 7 *A*). Importantly, very little pulse or tail currents could be measured from the nontransfected cells. The plot in Fig. 7 *B* is the voltage-dependent activation in the cells with $V_{1/2}$ = −11.6 mV and k = 9 mV (n = 9). These properties of HERG channel activation are similar to those previously reported elsewhere for HERG (Sanguinetti et al., 1995; Trudeau et al., 1995; Smith et al., 1996; Snyders and Chaudhary, 1996; Kiehn et al., 1996; McDonald et al., 1997; Zhou et al., 1998). K^+ selectivity of the transfected HERG channels is shown in Fig. 7 *C*. Reversal potential (E_{rev}) was determined by measuring I_T reversal in external recording solutions containing 1, 5.4, or 10 mM external K^+. E_{rev} averaged −112.5 ± 2.5 mV, −76.25 ± 1.25 mV, and −62.5 ± 2.5 mV, respectively, for $[K^+]_o$ = 1, 5.4, and 10 mM external K^+ (n = 12). The solid line in the figure is the fit of experimental data to

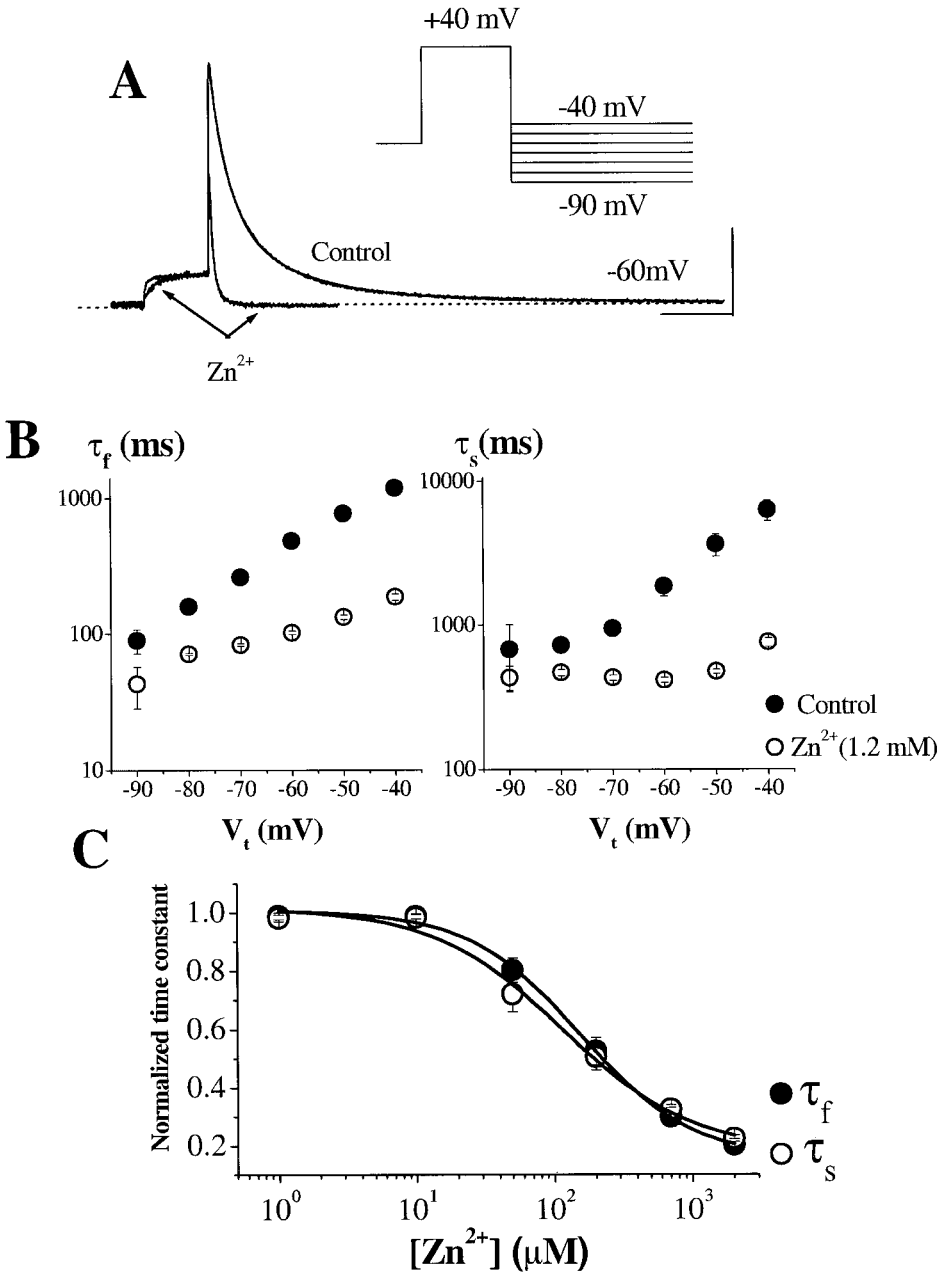

FIGURE 6 Effects of Zn^{2+} (1.2 mM) on tail current deactivation kinetics in oocytes. (*A*) Representative traces in control and in the presence of extracellular Zn^{2+}. The voltage protocol was the same as in Fig. 5 *A*. Tail currents have superimposed biexponential fits with time constants of 0.60 and 2.49 sec in control and 0.10 and 0.38 sec in the presence of Zn^{2+}. Calibration bars: 1 μA, 2 sec. (*B*) Voltage dependence of the fast (τ_{fast}; *left plot*) and the slow (τ_{slow}; *right plot*) time constants ($n = 4$). (*C*) The time constants (τ_{fast}, τ_{slow}) of tail current deactivation plotted as a function of extracellular proton concentration. The K_d values for τ_{fast}, τ_{slow}, respectively, 169 ± 35 μM and 145 ± 50 μM ($n = 7$). The lines represent the best fit of data to a modified Hill equation.

the Goldmann–Hodgkin–Katz equation, with the relative permeability of Na^+ to K^+ (α) of 0.007. The sensitivity to methanesulfonanilides (E-4031, dofetilide, and MK499) is a distinguishing characteristic of I_{Kr}/HERG channels. As shown in Fig. 7 *D*, HERG channels expressed in L929 cells were blocked by nanomolar concentrations of E-4031.

Voltage-dependent activation

The acidification effects on voltage-dependent activation of HERG channels in L929 cells are summarized in Fig. 8 ($n = 7$). Representative traces in control and during acidification ($pH_o = 6.4$) are shown Fig. 8 *A*. Control and test currents (I_P and I_T) were normalized to their respective maximum control value and plotted against V_P (Fig. 8, *B* and *C*). Acidification did not significantly shift $V_{1/2}$ or alter control k values ($n = 7$). I_P and I_T ($V_p = 0$ mV) were inhibited, respectively, by ~32% and 39%. At positive potentials, there was an apparent greater inhibition of I_T than of I_P. However, due to channel rectification, during which I_P becomes increasingly smaller in amplitude, it is possible that the ability to resolve any proton effects on current amplitude may be reduced. However, I_T measured at −60 (Vp > +10 mV), were significantly inhibited by approximately equal amounts (~28%) during acidification.

Current activation/deactivation

Two approaches were used to study proton effects on current activation in the L929 cells. First, τ_f and τ_s were

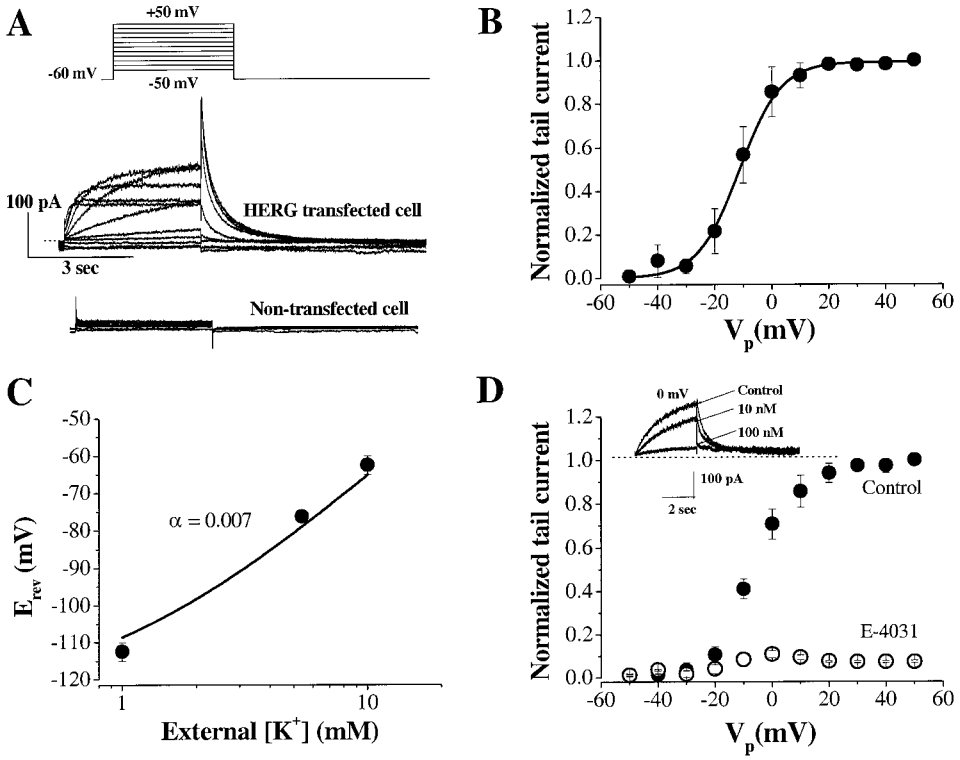

FIGURE 7 Biophysical and pharmacological properties of HERG channels stably transfected in L929 cells. (*A*) Currents recorded from a HERG transfected cell and from a control (nontransfected) cell. The voltage-clamp protocol is applicable for both cells. Currents were activated by 4-sec depolarizing pulses. Dotted line in this and subsequent figures represent zero current level. (*B*) Tail current amplitudes plotted against test potentials (n = 9). Tail currents were normalized to the maximum value in each experiment. (*C*) E_{rev} plotted as a function of $\log[K^+]_o$ (n = 12). The permeability of Na^+ relative to K^+ (α) was 0.007 and was obtained by fitting data points to the Goldmann–Hodgkin–Katz equation. (*D*) Sensitivity of the HERG channels to E4031. Inset represents current traces activated by depolarization to 0 mV in control and in the presence of 10 and 100 nM drug concentrations. The plot is the average data in three cells showing the effect of E4031 (100 nM) on tail current amplitude. Currents were normalized to the maximum control value in each cell.

estimated by directly fitting I_P at 0 mV (Zhou et al., 1998). Using this procedure, τ_f and τ_s of apparent activation were not significantly changed by acidification, averaging, respectively, 165 ± 37 ms and 985 ± 233 ms in control and 125 ± 20 ms and 695 ± 128 ms (n = 6) during acidification. Second, we exploited the ability to remove transiently

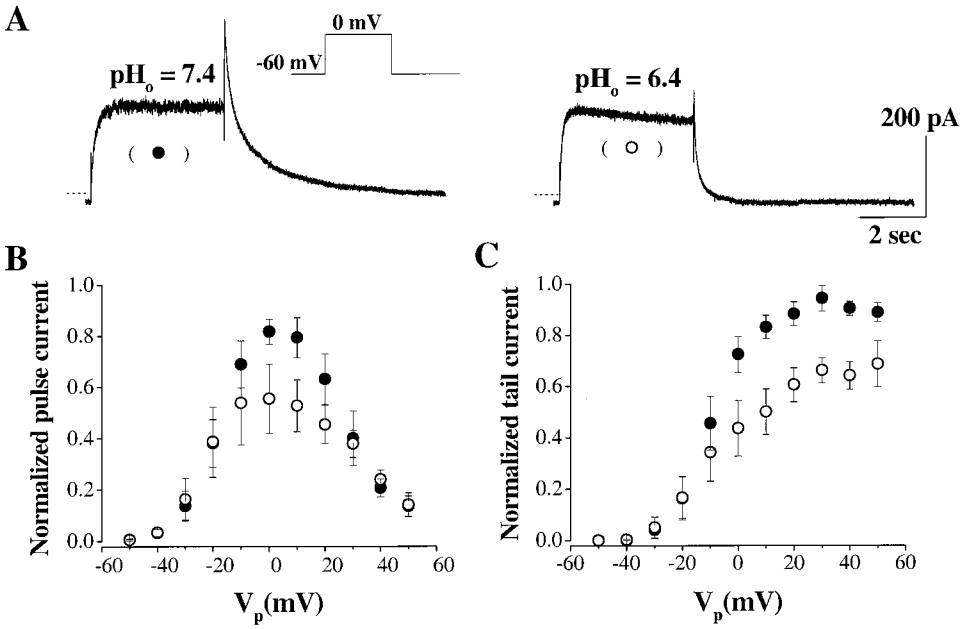

FIGURE 8 Effects of acidification (pH_o = 6.4) on the HERG current amplitude in L929 cells. (*A*) Currents recorded by depolarization to 0 mV (V_p) in control (pH_o = 7.4) and during acidification. (*B*) Acidification effects on pulse currents. (*C*) Acidification effects on tail currents. In *B* and *C*, currents were normalized to the maximum control value in each cell.

the rapid inactivation that occurs during activation to generate an envelope of pulse currents, the time course of which describes current activation. This enabled us to study activation at a more positive potential (+60 mV). The voltage protocol we used consisted of a three-pulse (P1–P3) paradigm (Fig. 9 *A*, *inset*): a depolarizing pulse (P1) of variable duration (Δt), a 10-ms hyperpolarizing pulse to −110 mV (P2), and another depolarizing pulse (P3). P3 was always applied to the same voltage as P1 but was fixed in duration (30 ms). A representative current trace obtained with the P1–P3 paradigm is shown in Fig. 9 *A*. Illustrated in Fig. 9 *B* is an envelope of peak P3 values that was generated as Δt was progressively increased. The superimposed broken line is a single exponential fit of the data. Fig. 9 *C* shows that the time constant of current activation was not significantly altered by the acidification, averaging 44 ± 6 ms in control and 45 ± 3 ms at $pH_o = 6.4$. Note, however, that current amplitude in the envelope (measured at 250 ms) was inhibited by 31 ± 0.1% ($n = 3$) during acidification. The inset in Fig. 9 *C* shows isochronal currents during P3 for control and during acidification. The traces (#10 in the envelope) were taken from the same cell as shown in Fig. 9 *B*.

To study proton effects on deactivation, currents were activated using a 300-ms duration V_P applied to +40 mV (HP = −60 mV). I_T was then measured on return to a range of potentials (Fig. 10). Given the previously reported $V_{1/2}$ for HERG channel inactivation, (−49 mV; Sanguinetti et al., 1995), some degree of inactivation is expected to overlap the deactivation process. However, the relatively fast kinetics of inactivation in this voltage range would suggest that deactivation was essentially a steady-state process and would not have a major effect on the analysis.

Traces of tail currents and superimposed biexponential fits are shown in Fig. 10 *A* for control and during acidification. Acidification effects on the relative amplitude of the fast component of the time constant is plotted in Fig. 10 *B*. As clearly demonstrated in Fig. 10, *C* and *D*, acidification had a major effect on tail current kinetics, speeding deactivation (τ_f) by approximately two fold or more. τ_f at V_t = −60 mV averaged 34 ± 4 ms for control and 17 ± 1 ms during acidification ($n = 3$). As was shown for HERG expressed in oocytes, the data in the L929 cell transfectants demonstrate that the deactivation process of the HERG channel is very sensitive to extracellular protons.

Onset and recovery of inactivation

Proton effects on the onset and recovery of inactivation were studied using voltage-clamp protocols similar to those previously described (Spector et al., 1996; Smith et al., 1996; Snyders and Chaudhary, 1996). The protocols are shown as insets in Fig. 11, *B* and *D*. Fig. 11 *A* shows selected traces (and monoexponential fits) in control ($pH_o = 7.4$) and during acidification ($pH_o = 6.4$) (test voltage = 0 mV). Currents were measured at the arrow in the protocol. The inset in the figure is a superimposition of traces in control and during acidification. To scale the traces, each was normalized to its maximum value. Fig. 11 *B* summarizes the results in three cells and shows that the relatively moderate acidification did not significantly alter the onset of inactivation. Similarly, the recovery process from channel inactivation was not significantly changed by the acidification. Currents were measured at the arrow in the protocol. The inset in the figure is a superimposition of traces in control and during acidification. For scaling, each trace was normalized to its maximum value. Fig. 11 *D* summarizes the results in three cells and shows that the

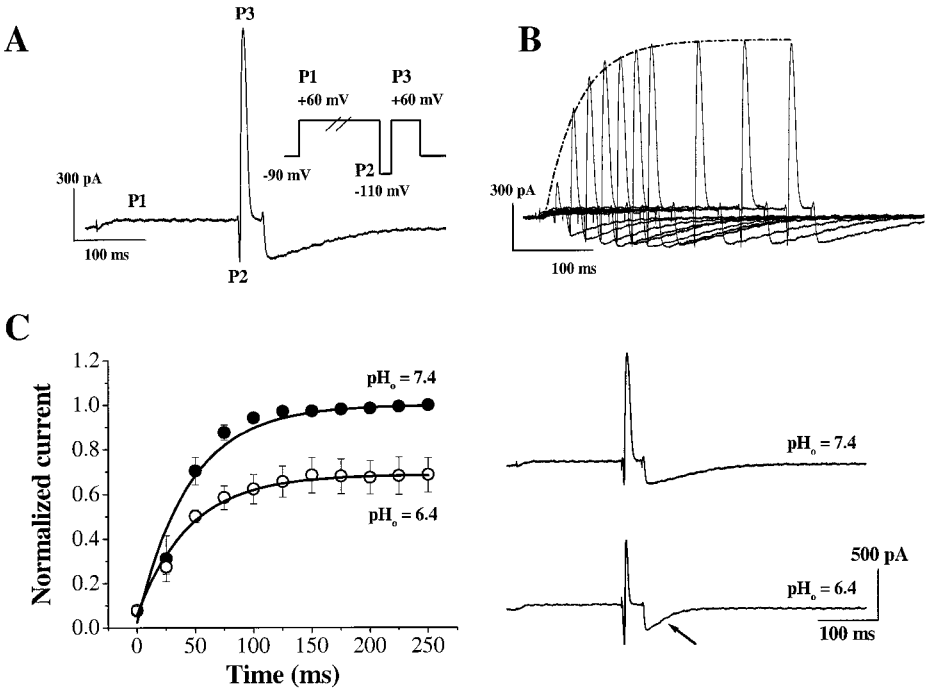

FIGURE 9 Acidification effects on kinetics of current activation in L929 cells. (*A*) A representative current trace and the P1–P3 paradigm used to study kinetics of current activation. The voltage protocol consisted of a depolarizing pulse (HP = −90 mV) to +60 mV (P1) of variable duration, a 10-ms hyperpolarizing pulse to −110 mV pulse (P2), and a depolarizing pulse to +60 mV (P3). P3 was applied for a fixed duration of 30 ms (see text for details). (*B*) An envelope of pulse currents at +60 mV generated using the peak current values of P3. Broken line is an exponential fit to peak P3 current values. (*C*) Time course of current activation determined by fitting the envelope of pulse currents ($n = 3$). The insets are isochronal currents for control and during acidification in one cell. The arrow highlights acidification effect on current deactivation.

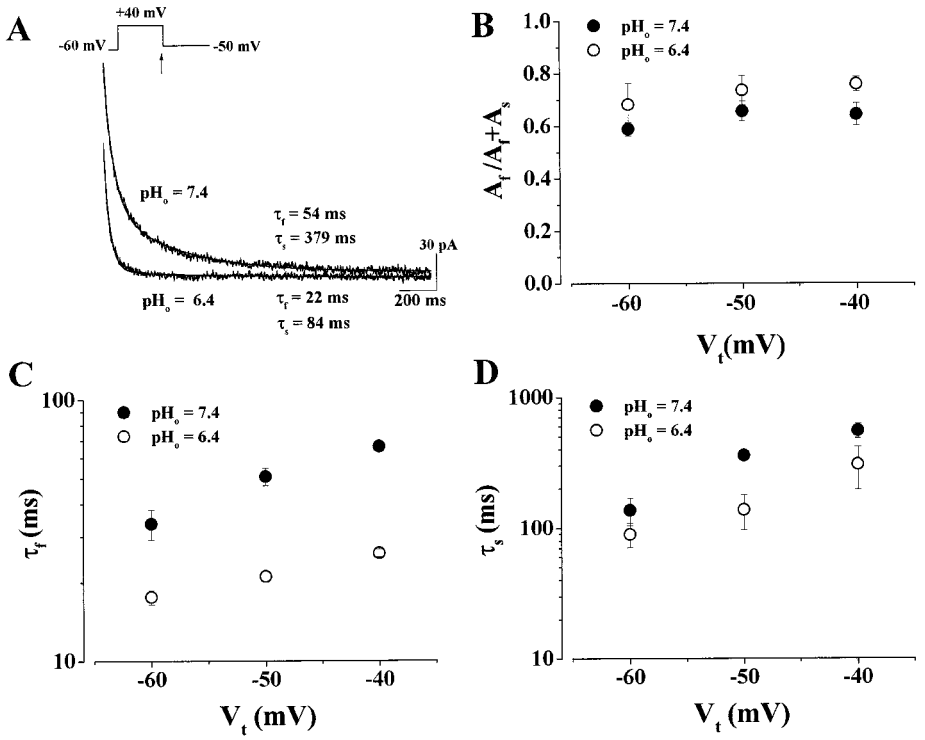

FIGURE 10 Effects of acidification on deactivation kinetics in L929 cells. Currents were activated by a 300-ms depolarizing step to +40 mV (holding potential = −60 mV) followed by hyperpolarization (V_t) to −40, −50, and −60 mV. (*A*) Tail currents and superimposed biexponential fits for control and during acidification, measured for deactivation at −50 mV. (*B*) Acidification effects on the relative amplitude of the fast component of current deactivation time constant. (*C*) Effects of acidification on the fast time constant of current deactivation (n = 3). (*D*) Effects of acidification on the slow time constant of current deactivation (n = 3).

acidification did not significantly alter recovery from the inactivation process. Note, nonetheless, the acceleration of a component of the current trace (Fig. 11 *C*, *inset*) which represents the proton effect on current deactivation.

DISCUSSION

We have investigated effects of protons and Zn^{2+} on HERG channels after expression in *Xenopus* oocytes and in the L929 cell line. Our major finding is that HERG channel deactivation is very sensitive to moderate changes in the pH of the cellular environment. Lowering of pH within the physiological range dramatically accelerated channel deactivation without shifting activation on the voltage axis or altering the time course of current activation or inactivation (onset and recovery). In oocytes expressing HERG, low pH and Zn^{2+} accelerated the kinetics of deactivation with apparent K_d values about one order of magnitude lower than for tail current inhibition. These data suggest that protons and Zn^{2+} directly interact with the HERG channel.

Limitations of study

In this study, a number of buffers were used to determine proton concentration effects on HERG currents. We would like to note that control experiments were not carried out to determine any direct buffer effects in the experiments. Nevertheless, there are reasons to conclude that the major proton effects are unlikely the direct consequence of the buffers used. First, the major cation effect is on current deactivation, with sensitivity that is one order of magnitude higher than for the effect on tail current inhibition. This effect was observed in the zinc experiments where only one buffer was used. Second, no changes in current amplitude were seen at pH > 6.4 where different buffers were used. Note also that a significant part of the dynamic range (pK_a = 7.0) of the buffer effect on deactivation occurs in the pH range where only one buffer (HEPES) was used (Fig. 5 *C*). Although it is possible that the buffers may have additional effects on HERG currents, our data, nevertheless, suggest that the changes in kinetics are primarily attributable to the effects of the cations under study.

A hallmark of the HERG is an overlap of channel activation by a rapid inactivation process. The experimental protocols, therefore, must be chosen carefully when studying inactivation. This is particularly so for experiments at physiological temperature, a condition that is expected to hasten the rates of the processes. We did not measure cation effects on inactivation kinetics in oocytes, given the inherent problems of voltage-clamp in the relatively large preparation. Proton effects on inactivation were carried out only in the L929 cells, in which the relatively small cell size (~22 pF) would have the advantage of improving voltage-clamp quality, resulting from reduced capacitive loading. HERG channel inactivation kinetics have been previously determined in mammalian cells under similar conditions (Zhou et al., 1998). We would like to point out that, although intracellular pH measurements were not carried out in the L929 cells, any changes in intracellular pH, however, would have been minor considering that appropriate nonpermeant buffers were used in the experiments. Consistent with this is the fact that we did not find significant changes

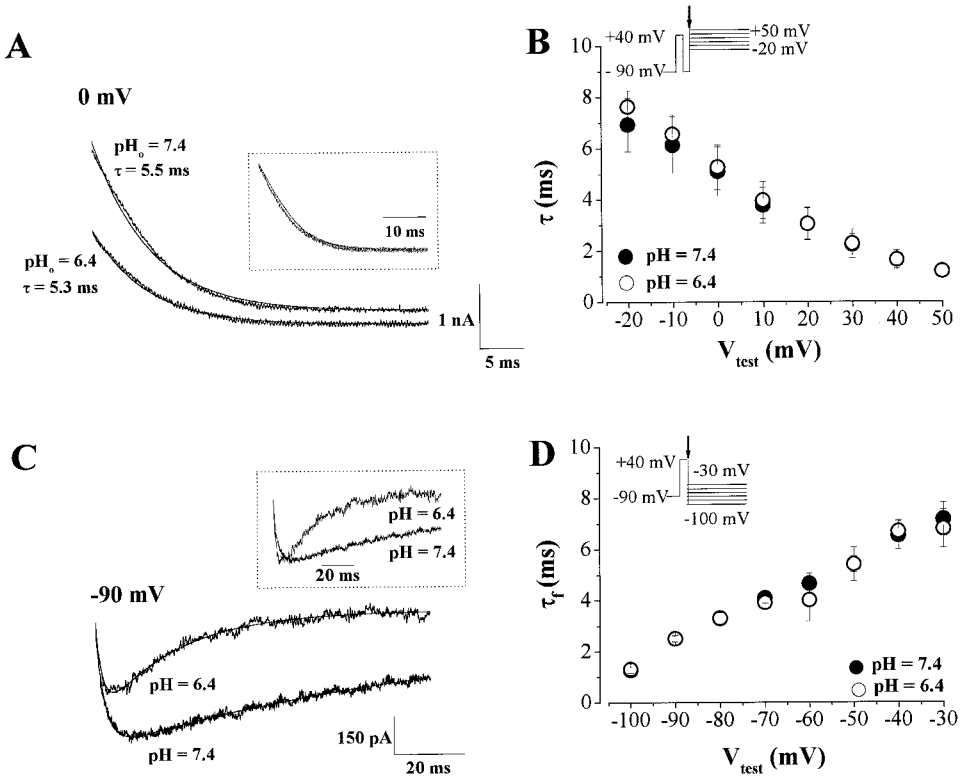

FIGURE 11 Acidification effects on the onset and recovery of current inactivation in L929 cells. (*A*) Inactivation onset at 0 mV (V_{test}) recorded in control and during acidification (pH_o = 6.4). Control and test traces have monoexponential fits superimposed. Note the effect of protons on current amplitude but not on kinetics. Inset is a superimposition of traces in control and during acidification. For scaling, each trace was normalized to its maximum value. (*B*) The voltage dependence of current inactivation onset, in control and during acidification (n = 3). (*C*) Currents recorded during recovery from inactivation in control and during acidification (V_{test} = −90 mV). Both current traces have biexponential fits superimposed. Inset is a superimposition of traces in control and during acidification. For scaling, each trace was normalized to its maximum value. Note that, whereas protons had no significant effect on the recovery process at the pH value, deactivation was accelerated (also, see arrow in Fig. 9 *C*, *inset*). (*D*) The voltage dependence of current recovery from inactivation, in control and during acidification (n = 3).

in the holding current during acidification, which would have indicated proton-induced membrane depolarization.

A consideration must be given also to the underlying theory in Eq. 6, which was used to estimate charge density. A key assumption is that the charges are in a uniformly smeared layer (Grahame, 1947). However, as was pointed out in a previous study (Peitzsch et al., 1995), Eq. 6 can be used to estimate "reasonably" charge densities that are more negative than $-0.16e$ nm^{-2}. Based on this, charge densities of $-1e$/270–900 Å^2 were reported for other potassium channels exogeneously expressed in *Xenopus* oocytes (Elinder et al., 1996). Therefore, our estimation of charge density ($-1e$/425 Å^2) using this procedure can be justified.

Modulatory effects of protons and Zn^{2+} on HERG currents in oocytes

Divalent cations have important regulatory effects on ion channels (reviewed in Hille, 1992). These effects were originally thought to result from the neutralization of negative charges on the cell membrane, thereby creating a steeper voltage gradient across the membrane and shifting channel gating parameters to more positive voltages (Frankenhaeuser and Hodgkin, 1957). However, studies have since presented evidence that cations can also directly interact with ion channels to cause blockade or to regulate gating properties (Agus et al., 1991; Coulter et al., 1995; Paquette et al., 1998; Ho et al., 1998; Elinder and Århem, 1994).

Our results demonstrate that protons and Zn^{2+} have important modulatory effects on HERG channels. In oocytes expressing HERG, protons and Zn^{2+}, at their respective K_d values, shifted steady-state activation, slowed the time course of current activation, and accelerated current deactivation. These effects suggest a shift of gating parameters to more positive potentials on the voltage axis. During relatively moderate extracellular acidification (pH_o = 6.4), protons did not significantly affect the pulse current amplitude or time course, but accelerated current deactivation and inhibited the tail current amplitude by 11%. It is a significant observation that low pH (and Zn^{2+}) accelerated the kinetics of deactivation of HERG channels with sensitivity that is one order of magnitude higher than for current inhibition. Thus, the K_d values for tail current inhibition versus acceleration of deactivation were, respectively, 1.8 μM (pK_a = 5.8) and 0.1 μM (pK_a = 7.0). These results

suggest that there is a direct proton effect on HERG channels. We speculate that protons (and Zn^{2+}) directly interact with the channel in a manner that channel closing rates are preferentially modulated. A direct interaction of cations with the HERG channel is consistent with the reported direct effects of transition metals on I_{Kr} in isolated rabbit ventricular cells. Paquette et al. (1998) showed that cadmium, nickel, cobalt, and manganese shifted current activation and accelerated tail current deactivation. Also, it was demonstrated that Zn^{2+} blocked I_{Kr} but did not shift the midpoint of channel activation. The +21 mV shift in HERG current activation in oocytes, in comparison to results in ventricular cells, may reflect the oocyte membrane properties or may be due to differences resulting from a native channel versus a cloned, exogenously expressed channel. For instance, no ancillary subunits were coexpressed or transfected with HERG in our study.

Modulatory effects of protons on HERG currents in L929 cells

The data on proton effects in L929 cells provide information on the cation effects in a mammalian cell environment at physiological temperature. Because there were no previous reports of HERG properties in this cell line, it was imperative to profile channel characteristics before determining any proton effects. Several previous studies had established a unique biophysical and pharmacologic profile for HERG/I_{Kr}. Rapid channel activation is overlapped by a fast inactivation process (Wang et al., 1994; Ono and Ito, 1995; Sanguinetti et al., 1995; Smith et al., 1996; McDonald et al., 1997; Zhou et al., 1998). Moreover, the channels are selectively sensitive to the methanesulfonalilides (Sanguinetti and Jurkiewicz, 1990; Snyders and Chaudhary, 1996; Liu and Antzelevitch, 1995). After transfection, HERG channels retained their biophysical properties, including a relatively high K^+-selectivity ($\alpha = 0.007$). Furthermore, the channels were almost completely blocked by 100 nM E-4031. This sensitivity is within the range previously reported for the methanesulfonanilides on HERG/I_{Kr} (IC_{50} = 4–31 nM; Carmeliet, 1992; Yang et al., 1994; Snyders and Chaudhary, 1996; Spector et al., 1996; Liu et al., 1996; Zhou et al., 1998).

Experiments on HERG channels in the L929 cells, in comparison to those in oocytes, showed that relatively moderate acidification of the extracellular space ($pH_o = 6.4$) had a significant effect on HERG channel currents, inhibiting both pulse and tail current amplitudes, respectively, by 32% and 39% of control values. Data in the oocyte experiments showed little or no effect on pulse current amplitude and an 11% block of tail current amplitude for a similar change in extracellular pH. Results in both expression systems, however, demonstrate that the proton effects were not accompanied by any significant shifts in steady-state activation at this pH. The smaller amount of tail current inhibition in the oocyte experiments compared to that in the L929 cells (11% versus 39%) may reflect the temperature and/or cell environment effects on the regulatory mechanism. Unpublished data from our laboratory showed that acidification to pH_o = 6.4 inhibited HERG tail currents by approximately 15% in the L929 cells maintained at room temperature. Our data also show that relatively moderate acidification does not have any significant effect on the channel inactivation process. In contrast, protons profoundly modified current deactivation, accelerating the process by as much as 2–3 fold, for this moderate change in pH_o.

HERG/I_{Kr} channel gating has not been sufficiently examined; however, the current activation appears to involve sequential transitions between closed (C), open (O), and inactivated (I) states (Trudeau et al., 1995; Liu et al., 1996, Wang et al., 1997; Ho et al., 1998). Furthermore, there are reports of sigmoidal delay in current activation, suggestive of multiple closed states (Liu et al., 1996; Wang et al., 1997). The predominant effect on current deactivation would suggest that protons (and Zn^{2+}), potentially could bind or interfere with any of the C, O, and I states, but primarily regulate transitions between O and C, i.e., channel deactivation. Clearly, single-channel data will be required to firmly establish this.

Possible site(s) of interaction of extracellular protons and Zn^{2+}

Recently, the effects of strontium on five cloned delayed rectifiers were studied in oocytes to determine the ion-induced shifts of channel open probability. Charge density estimates for the channels were reported as $-1e/270$–900 Å^2 (Elinder et al., 1996). Our charge density estimates of $-1e/425$ Å^2 show that HERG is most similar to the Kv 1.6 with an estimated charge density of $-1e/490$ Å^2. Studies have identified cation binding sites in the ancestrally related cyclic nucleotide-gated (cNG) and *Shaker* potassium channels (Heginbotham et al., 1992; Root and MacKinnon, 1993, 1994; Ellinor et al., 1995; Chen et al., 1996). In the investigations, evidence was provided for pore-region acidic residues such as Glu and Asp. A pore region Glu in an equivalent position of the Ca^{2+} channel has also been suggested as the molecular mechanism of channel block by cations (Chen et al., 1996). HERG is closely related to the cNG and *Shaker* channel proteins (Warmke and Ganetzky, 1994), and a comparison of their putative pore regions and the surrounding residues shows that HERG has a number of acidic residues as well as two histidine residues (His^{578} and His^{587}). Importantly, HERG has an asparagine residue (Asn^{629}) in an equivalent position as Asp^{447} in *Shaker* or Glu^{363} in the cNG channel. Arguably, any of these acidic residues, or the histidines, may be the molecular determinant of cation sensitivity of HERG channels. Structure–function experiments involving site-directed mutagenesis will be required to determine the relevant residues.

Physiological implications

The identification of HERG as one locus for familial long Q-T syndrome established the role of the gene in the cardiac excitation process, and it is generally assumed that HERG is the primary channel α subunit mediating I_{Kr} in several species (Curran et al., 1995; Sanguinetti et al., 1995). If the proton-sensitivity of HERG channels we report in this study is similar to that in vivo, the channel properties will be altered under ischemic conditions following an increase in proton concentration. Ca^{2+} and Na^+ channels are also thought to play important roles in modulating cell electrical properties during ischemia (Krafte and Kass, 1988; Zhang and Siegelbaum, 1991). The observation that HERG current inhibition was reduced by 17% in the presence of 10 mM external potassium is significant, given that such an increase in extracellular potassium may be observed in ischemia. Additionally, we have shown that the acidification-induced HERG channel closing has a relatively high pK_a (~7.0). Taken together, these properties may suggest an even greater involvement of HERG in the myocardium under the ischemic conditions. Specifically, the faster closing should reduce the total amount of K^+ loss. Such a role has been suggested for the HIR K^+ channel (Coulter et al., 1995), although the precise molecular mechanisms involved may be very different for the two channels.

Our results also have important implications in pacemaker cells. Recovery from inactivation and deactivation are thought to be important determinants of the total outward currents for repolarization in cells expressing HERG. In rabbit pacemaker cells (Ono and Ito, 1995; see also Fig. 10 *C* in Zhou et al., 1998), diastolic depolarization was shown to reflect current deactivation. In this regard, the finding that the deactivation of HERG channels is particularly sensitive to extracellular acidification may have important physiological consequences. In the myocardium, for example, the ischemia-induced increase in extracellular proton concentration to pH_o of ~6.8 would have no significant effect on HERG channel inactivation (onset or recovery) but will profoundly accelerate channel deactivation, consequently limiting the total outward current during repolarization. Potentially, these effects would modify action potential duration in general as well as define the trajectory of diastolic depolarization in pacemaker cells.

In conclusion, we have shown that HERG channel properties are significantly regulated by moderate changes in the pH of the cellular environment. Lowering of pH within the physiological range dramatically accelerated channel deactivation without significantly altering the time course of activation or of inactivation. Overall, our results suggest that protons and Zn^{2+} directly interact with HERG channels to regulate channel function.

We wish to thank Drs. T. Begenisich and J. Sullivan for their advice and comments on this manuscript, and we would like to thank Dr. J. Beaumont for assisting in the charge density calculations. We also wish to thank Wanda Coombs, Christine Burrer, Meg Flanagan, Marta Mastroianni, and Laura Hofmann for their technical support.

REFERENCES

Agus, Z. S., I. D. Dukes, and M. Morad. 1991. Divalent cations modulate the transient outward current in rat ventricular myocytes. *Am. J. Physiol.* 261:C310–C318.

Anumonwo, J. M. B., M. Delmar, and J. Jalife. 1990. Electrophysiology of single heart cells from the rabbit tricuspid valve. *J. Physiol. Lond.* 425:145–167.

Anumonwo, J. M. B., L. C. Freeman, W. M. Kwok, and R. S. Kass. 1992. Delayed rectification in single cells isolated from guinea pig sinoatrial node. *Am. J. Physiol.* 262:H921–H925.

Bard, Y. 1974. Nonlinear Parameter Estimation. Academic Press, New York.

Barhanin, J., F. Lesage, E. Guillemare, M. Fink, M. Lazdunski, and G. Romey. 1996. K_VLQT1, and I_{sK} (minK) proteins associate to form the I_{Ks} cardiac potassium current. *Nature*. 384:78–80.

Barrio, L. C., T. Suchyma, T. Bargiello, L. X. Xu, R. S. Roginski, M. V. L. Bennett, and J. Nicholson. 1991. Gap junctions formed by connexins 26 and 32 alone and in combination are differently affected by applied voltage. *Proc. Natl. Acad. Sci. USA*. 88:8410–8414.

Campbell, D. L., R. L. Rasmusson, and H. C. Strauss. 1992. Ionic current mechanisms generating vertebrate primary pacemaker activity at the single cell level: an integrative view. *Ann. Rev. Physiol.* 54:279–302.

Carmeliet, E. 1992. Voltage- and time-dependent block of the delayed K^+ current in cardiac myocytes by dofetilide. *J. Pharmacol. Exp. Ther.* 262:809–817.

Cascio, W. E., T. A. Johnson, and L. S. Gettes. 1995. Electrophysiologic changes in ischemic ventricular myocardium. I. Influence of ionic, metabolic, and energetic changes. *J. Cardiovasc. Electrophysiol.* 6:1039–1062.

Chen, X.-H., I. Bezprozvanny, and R. W. Tsien. 1996. Molecular basis of proton block of L-type Ca^{2+} channels. *J. Gen. Physiol.* 108:363–374.

Coulter, K. L., F. Perier, C. M. Radeke, and C. A. Vandenberg. 1995. Identification and molecular localization of a pH-sensing domain for the inward rectifier potassium channel HIR. *Neuron.* 15:1157–1168.

Curran, M. E., I. Splawski, K. W. Timothy, G. M. Vincent, E. D. Green, and M. T. Keating. 1995. A molecular basis for cardiac arrhythmia: HERG mutations cause long QT syndrome. *Cell.* 80:795–803.

De Biasi, M., J. A. Drewe, G. E. Kirsch, and A. M. Brown. 1993. Histidine substitution identifies a surface position and confers Cs^+ selectivity on a K^+ pore. *Biophys. J.* 65:1235–1242.

Ebihara, L. 1996. *Xenopus* connexin38 forms hemi-gap-junctional channels in the nonjunctional plasma membrane of *Xenopus* oocytes. *Biophys. J.* 71:742–748.

Ek-Vitorin, J. F., G. Calero, G. E. Morley, W. Coombs, S. M. Taffet, and M. Delmar. 1996. pH regulation of connexin43: molecular analysis of the gating particle. *Biophys. J.* 71:1273–1284.

Elinder, F., and P. Århem. 1994. Effects of gadolinium on ion channels in the myelinated axon of *Xenopus laevis*: four sites of action. *Biophys. J.* 67:71–83.

Elinder, F., M. Madeja, and P. Århem. 1996. Surface charges of K channels. Effects of strontium on five cloned channels expressed in *Xenopus* oocytes. *J. Gen. Physiol.* 108:325–332.

Ellinor, P. T., J. Yang, W. A. Sather, J. F. Zhang, and R. W. Tsien. 1995. Ca^{2+} channel selectivity at a single locus for high-affinity Ca^{2+} interactions. *Neuron.* 15:1121–1132.

Frankenhaeuser, B., and A. L. Hodgkin. 1957. The action of calcium on potassium conductance of squid axons. *J. Physiol. Lond.* 137:218–244.

Gilly, W. F., and C. M. Armstrong. 1982. Divalent cations and the activation kinetics of potassium channels in squid giant axons. *J. Gen. Physiol.* 79:965–996.

Gintant, G. A., I. S. Cohen, N. B. Datner, and R. P. Kline. 1992. Time-dependent outward currents in the heart. *In* The Heart and Cardiovascular System, 2nd ed. H. Fozzard, editor. Raven Press, Ltd., New York. 1121–1169.

Goldmann, D. E. 1943. Potential, impedance and rectification in membranes. *J. Gen. Physiol*. 27:37–60.

Grahame, D. C. 1947. The electrical double layer and the theory of electrocapillarity. *Chem. Rev.* 41:441–501.

Hamill, O. P., A. Marty, E. Neher, S. Sakmann, and F. J. Sigworth. 1981. Improved patch-clamp techniques for high-resolution current recording from cells and cell-free membrane patches. *Pflug. Archiv.* 391:85–100.

Heginbotham, L., T. Abramson, and R. MacKinnon. 1992. A functional connection between the pores of distantly related ion channels as revealed by mutant K^+ channels. *Science.* 258:1152–1155.

Hille, B. 1992. Ionic Channel of Excitable Membranes, 2nd ed. Sinauer Associates, Sunderland, MA.

Ho, W., I. Kim, C. O. Lee, and Y. E. Earm. 1998. Voltage-dependent blockade of HERG channels expressed in *Xenopus* oocytes by external Ca^{2+} and Mg^{2+}. *J. Physiol. Lond.* 507:631–638.

Hodgkin, A. L, and B. Katz. 1949. The effect of sodium ions on the electrical activity of the giant axon of the squid. *J. Physiol. Lond.* 108:37–77.

Horta, J., S. M. Taffet, M. Delmar, J. Jalife, and J. M. B. Anumonwo. 1996. Regulation of HERG-induced current (I_{Kr}) by protons. *Biophys. J.* 70: A277 (Abstr.).

Kiehn, J., A. E. Lacerda, B. Wible, A. M. Brown. 1996. Molecular physiology and pharmacology of HERG. *Circulation.* 94:2572–2579.

Krafte, D. S., R. S. Kass. 1988. Hydrogen ion modulation of Ca channel current in cardiac ventricular cells. *J. Gen. Physiol.* 91:641–657.

Kurachi, Y. 1982. The effects of intracellular protons on the electrical activity of single ventricular cells. *Pfluegers Arch.* 394:264–270.

Liu, D.-W., and C. Antzelevitch. 1995. Characteristics of the delayed rectifier current (I_{Kr} and I_{Ks}) in canine ventricular epicardial, midmyocardial, and endocardial myocytes. *Circ. Res.* 76:351–365.

Liu, S., R. L. Rasmusson, D. L. Campbell, S. Wang, and H. C. Strauss. 1996. Activation and inactivation kinetics of an E-4931-sensitive current from single ferret atrial myocytes. *Biophys. J.* 70:2704–2715.

McDonald, T. V., Z. Yu, Z. Ming, E. Palma, M. B. Meyers, K.-W. Wang, S. A. N. Goldstein, and G. I. Fishman. 1997. A minK-HERG complex regulates the cardiac potassium current I_{Kr}. *Nature.* 388:289–292.

McAllister, R. E., D. Noble, and R. W. Tsien. 1975. Reconstruction of the electrical activity of cardiac Purkinje fibres. *J. Physiol. Lond.* 251:1–59.

Morley, G. E., S. M. Taffet, and M. Delmar. 1996. Intramolecular interactions mediate pH regulation of connexin43 channels. *Biophys. J.* 70: 1294–1302.

Ono, K, and H. Ito. 1995. Role of rapidly activating delayed rectifier K^+ current in sinoatrial node pacemaker activity. *Am. J. Physiol.* 263: H453–H462.

Paquette, T., J. R. Clay, A. Ogbaghebriel, and A. Shrier. 1998. Effects of divalent cations on the E-4031-sensitive repolarization current, I_{Kr}, in rabbit ventricular myocytes. *Biophys. J.* 74:1278–1285.

Peitzsch, R. M., M. Eisenberg, K. A. Sharp, and S. McLaughlin. 1995. Calculation of the electrostatic potential adjacent to model phospholipid bilayers. *Biophys. J.* 68:729–738.

Root, M. J., and R. MacKinnon. 1994. Two identical non interacting sites in an ion channel revealed by proton transfer. *Science.* 265:1852–1865.

Sanguinetti, M. C., M. E. Curran, A. Zhou, J. Shen, P. S. Spector, D. L. Atkinson, and M. T. Keating. 1996. Coassembly of K_VLQT1 and minK (IsK) proteins to form cardiac I_{Ks} potassium channel. *Nature*. 384: 80–83.

Sanguinetti, M. C., C. Jiang, M. E. Curran, M. T. Keating. 1995. A mechanistic link between an inherited and an acquired cardiac arrhythmia: HERG encodes the IKr potassium channel. *Cell.* 81: 299–307.

Sanguinetti, M. C., and N. K. Jurkiewicz. 1990. Two components of cardiac delayed rectifier K^+ current. *J. Gen. Physiol.* 96:195–215.

Schönherr, R., and S. H. Heinemann. 1996. Molecular determinants for activation and inactivation of HERG, a human inward rectifier potassium channel. *J. Physiol. Lond.* 493:635–642.

Smith, P. L., T. Baukrowitz, and G. Yellen. 1996. The inward rectification mechanism of the HERG cardiac potassium channel. *Nature.* 379: 833–836.

Snyders, D. J., and A. Chaudhary. 1996. High affinity open channel block by dofetilide of HERG expressed in human cell line. *Mol. Pharmacol.* 49:949–955.

Spector, P. S., M. E. Curran, A. Zhou, M. T. Keating, and M. C. Sanguinetti. 1996. Fast inactivation causes rectification of the I_{Kr} channel. *J. Gen. Physiol.* 107:611–619.

Trudeau, M. C., J. W. Warmke, B. Ganetzky, G. A. Robertson. 1995. HERG, a human inward rectifier in the voltage-gated potassium channel family. *Science.* 269:92–95

Wang, Z., B. Fermini, and S. Nattel. 1993. Delayed rectifier outward current and repolarization in human atrial myocytes. *Circ. Res.* 73: 276–285.

Wang, S., S. Liu, M. J. Morales, H. C. Strauss, and R. L Rasmusson. 1997. A quantitative analysis of the activation and inactivation kinetics of HERG expressed in *Xenopus* oocytes. *J. Physiol. Lond.* 502:45–60.

Watson, C. L., and M. R. Gold. 1995. Effect of intracellular and extracellular acidosis on sodium current in ventricular myocytes. *Am. J. Physiol.* 268: H1749–H1756.

Warmke, J. W., and B. Ganetzky. 1994. A family of potassium channel genes related to *eag* in *Drosophila* and mammals. *Proc. Natl. Acad. Sci. USA.* 91:3438–3442.

Yang, T., M. S. Wathen, A. Filipe, M. M. Tamkun, D. J. Snyders, and D. M. Roden. 1994. K^+ currents and K^+ channel mRNA in cultured atrial cardiac myocytes (AT-1 cells). *Circ. Res.* 75:870–878.

Yatani, A., A. M. Brown, and N. Akaike. 1984. Effect of extracellular pH on sodium current in isolated, single rat ventricular cells. *J. Membrane Biol.* 78:163–168.

Zhang, J. F., and S. A. Siegelbaum. 1991. Effects of external protons on single cardiac sodium channels form guinea pig ventricular myocytes. *J. Gen. Physiol.* 98:1065–1083

Zhou, W., and S. W. Jones. 1996. The effects of external pH on calcium channel currents in bullfrog sympathetic neurons. *Biophys. J.* 70: 1326–1334.

Zhou, Z., Q. Gong, B. Ye, Z. Fan, J. Makielski, G. Robertson, and C. T. January. 1998. Properties of HERG channels stably expressed in HEK 293 cells studied at physiological temperature. *Biophys. J.* 74:230–241.